REVIEW ARTICLE

Terahertz phonon polariton imaging

Qiang Wu, **Qing-Quan Chen**, **Bin Zhang**, **Jing-Jun Xu**[†]

Key Laboratory of Weak Light Nonlinear Photonics (Ministry of Education), TEDA Applied Physics School and
School of Physics, Nankai University, Tianjin 300457, China

E-mail: [†]jjxu@nankai.edu.cn

Received January 10, 2013; accepted February 2, 2013

In this article, we primarily review the time-resolved imaging of THz phonon polariton, which is generated by femtosecond laser in ferroelectric crystal. We pay more attention to the imaging in thin crystal, which can be used as an integration platform for terahertz-optics or terahertz-electrics. The imaging techniques, which can get quantitatively in-focus time-resolved images, are introduced in more detail. They have made enormous progress in recent years, and are powerful tools for the research of phonon polariton, optics, and THz wave. We also briefly introduce the generation principle and general propagation properties of THz phonon polariton.

Keywords phonon polariton, terahertz wave, time-resolved imaging, femtosecond laser, ferroelectric crystal

PACS numbers 71.36.+c, 42, 42.30.-d, 42.65.Re, 42.82.-m, 77.84.-s

Contents

1 Introduction

Phonon polariton is a result of the coupling of an infrared photon with a transverse optic phonon (polar lattice vibration). It is a quasi-particle with partly electromagnetic and partly mechanical energy, which travels at light-like speed through the host [1, 2]. In another view, phonon polariton is the internal degrees of freedom of the substrate, which is excited by an external perturbation [3, 4].

In 1950s, Kun Huang first dealt with the elementary excitation, the coupling of electromagnetic wave and TO phonon, in an isotropic diatomic ionic crystal and predicted the existence of polariton [1, 5]. Later, Hopfield first named this kind of elementary excitation as polariton [6, 7]. Now the word "polariton" is widely used, which refers to the coupling of electromagnetic waves and polarization waves induced by elementary excitations, or quasi-particles consisting of photons and matter excitations [8]. Since there are a variety of elementary excitations in solids which can be coupled to the photons, there are also a lot of polariton species. For example, spin waves in ferromagnetic crystals can couple to electromagnetic wave to form magnon-polaritons [9]; Electron–hole excitations also can form exciton-polaritons [6, 10] or exciton-polariton microcavities [11–13]. In recent years, surface plasmon polaritons (SPPs), surface plasmons coupled with photons, have been experiencing a rapid increase of attention because of the amazing properties for nanophotonics [14].

For the research of phonon polariton, the discovery and early research have been conducted by means of inelastic light scattering spectroscopy [7, 15]. Thanks a lot to the development of laser technology, in 1980s, Aus-

ton and coworkers generated and detected the phonon polariton in ferroelectric crystal using femtosecond laser [16–20]. The frequencies of this kind of phonon polariton are in the range from hundreds of gigahertz to several terahertz (THz). In the case of the crystals typically used in our work, LiNbO$_3$ and LiTaO$_3$, the frequencies most easily observed are from 0.1 to 4 terahertz. Then, this method is widely used for the generation of terahertz wave for the application of terahertz spectroscopy or high speed signal processing. In recent years, it is especially used for the generation of high power terahertz wave and nonlinear terahertz spectroscopy [21–24].

On the other hand, a more visualized technique, spatiotemporal imaging for phonon polariton [25, 26] was developed to fully characterize the collective vibrational response travelling at light-like speeds through the sample. This powerful tool makes it possible to coherent control over lattice vibrational waves. Spatiotemporal imaging is also necessary for the research of the terahertz integration platform using ferroelectric crystals. In an on-chip platform, the information of terahertz wave generation, propagation, controlling, detection, and spectroscopic analysis can be fully integrated just in a thin crystal and acquired through the spatiotemporal imaging [27–29].

In this review, we present time-resolved imaging of THz phonon polariton in ferroelectric crystal. In Section 2, we briefly introduce the generation principle of THz phonon polariton by femtosecond laser in ferroelectric crystal. In Section 3, we show the propagation properties of THz phonon polariton in bulk and thin crystal and the time-resolved imaging techniques. We pay more attention to the thin crystal, especially to subwavelength waveguide, which can be used as an integration platform of THz phonon polariton. In Section 4, we introduce the properties of generation and propagation of THz phonon polariton in a subwavelength, anisotropic LiNbO$_3$ crystal waveguide. In the last section, we give a summary and perspectives.

2 Generation of THz phonon polariton in ferroelectric crystal by femtosecond laser

The general theory of phonon polariton has been studied for decades. In this review, we just focus on those in ferroelectric crystal, typically LiNbO$_3$ and LiTaO$_3$, generated by femtosecond laser. These theories have also been developed for some years [18, 20, 30–33]. The reasons of choice of LiNbO$_3$ and LiTaO$_3$ is that they can produce high power terahertz wave with tunable central wavelength and bandwidth and at the same time these crystals can be the on-chip platform to control or guide

THz waves. Moreover, they have large nonlinear optical coefficients and electro-optic coefficients, which make interconversion between terahertz frequencies and optical frequencies or electrical signal possible. Figure 1 shows some LiNbO$_3$ crystals with different doping, which are produced by Nankai University.
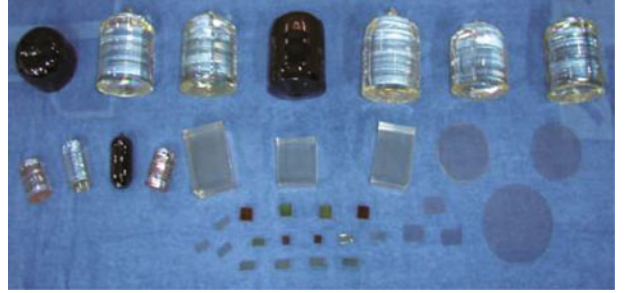

Fig. 1 Lithium niobate crystals produced by Nankai University.

First, we assume that phonon polariton works in the linear regime, although the nonlinear effects of THz phonon polariton are more useful and becoming more and more of interest. Then the model of ion motion in the crystal is essentially an oscillator that undergoes transverse vibrations when driven by an external electromagnetic field. The vibrated oscillators radiate electromagnetic waves which can be coupled to the lattice vibration wave to result in the phonon polariton. Second, we derive this coupling by a microscopic model using Maxwell's equations to derive the optical properties of phonon polariton. The derivations closely follow those given previously by Kun Huang. And we have to point out that LiNbO$_3$ and LiTaO$_3$ are of trigonal symmetry instead of cubic symmetry, so some derivation processes have to be adapted [27, 34, 35].

The phonon polariton equations are summarized as

$$\ddot{Q} + \Gamma\dot{Q} - b_{11}Q = b_{12}E \tag{1}$$

$$\left(\nabla^2\vec{A} - \frac{1}{c_0^2/\varepsilon_{\omega\to\infty}}\ddot{\vec{A}}\right) = -\mu_0\omega_{\text{TO}}\sqrt{\varepsilon_0(\varepsilon_{\omega\to 0} - \varepsilon_{\omega\to\infty})}\dot{\vec{Q}} \tag{2}$$

Here Q is the phonon normal mode displacement, E is the macroscopic electric field, and b coefficients are constants characteristic of the substance and direction relative to the optic axis of the uniaxial crystal. Phenomenological damping term Γ is introduced for the interactions among different eigen modes of lattice vibrations. $\vec{A}$ is a vector potential and we assume a non-magnetic material $\mu_0\vec{H} = \nabla \times \vec{A}$. ε_0 and μ_0 are the permittivity and the permeability of free space. $\varepsilon_{\omega\to 0}$ and $\varepsilon_{\omega\to\infty}$ are the dielectric constants in low and high frequency limits. ω_{TO} is the transverse optic (TO) phonon frequency.

For THz phonon polariton produced by femtosecond laser, a driving force from Impulsive Stimulate Raman

Scattering (ISRS) [30, 36] should be put into the phonon polariton equations

$$\ddot{Q} + \Gamma\dot{Q} - b_{11}Q = b_{12}E + F_{ISRS} \qquad (3)$$

So the properties of THz phonon polariton, such as central wavelength, wavelength bandwidth, can be changed by the properties of femtosecond laser pulse and the beam profile through ISRS. It is useful for the generation and control of THz phonon polariton wave.

A focused femtosecond laser beam by a cylindrical lens to a line or by a spherical lens to a point in the crystal will produce broadband, roughly single-cycle, phonon polariton wave. There are also some other methods to produce narrowband wave for high intensity, multi-oscillation of electromagnetic wave, or tunable central wavelength [22, 23, 37]. Because broadband waves are widely used for THz phonon polariton imaging, in this review we pay more attention to broadband THz phonon polariton.

From the normal dispersion equations of phonon polariton, we can get the dispersion curves of LiNbO$_3$, as shown in Fig. 2. The blue curves are the upper and lower branches of the dispersion. For the imaging, in most cases, the frequencies are below 2 terahertz. Although the behavior is very light-like here, some of the energy of phonon polariton is also stored in the ionic displacement.
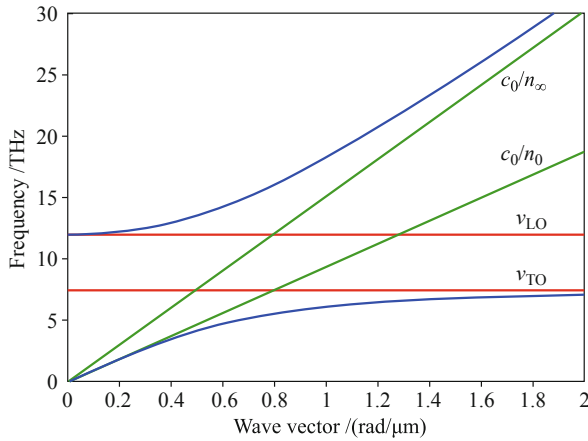

Fig. 2 Dispersion curves of the phonon polariton in LiNbO$_3$. The blue curves are the upper and lower branches, respectively. ν_{TO} and ν_{LO} are the resonance frequencies of the lowest transverse and longitudinal optic phonon mode, respectively. The green lines describe the dispersion of uncoupled optical radiation.

3 Propagation and imaging of THz phonon polariton in ferroelectric crystal

From our experience or intuition, when an electromagnetic wave is generated in a crystal by a laser, the produced electromagnetic wave will propagate collinearly with the pump beam, for example frequency doubling effect. But after THz phonon polariton waves are pro-

duced in ferroelectric crystals by femtosecond laser pulses through ISRS, they are in the case of phase matched in lateral directions, with the largest wavevector components perpendicular to the optical beam path for the reason of Cherenkov radiation effect [16, 17, 38, 39]. This key property makes it possible to obtain the time-resolved images of the field envelope, generation and propagation of THz phonon polariton.

3.1 Cherenkov radiation cone

Considering a focused femtosecond laser pulse propagates through a thick piece of LiNbO$_3$, as shown in Fig. 3, the pump is only acting in a small region of the crystal at any given instant in time. For a 100 fs pump pulse, it is only about 13 microns long inside the crystal. So the pump pulse produces a series of THz phonon polaiton waves along the propagation direction from the input face of the crystal to the output face. Since the pump pulse travels through the crystal significantly faster than the produced THz radiation (with a double speed for the difference of refractive indices), this will produce a Cherenkov cone. The angel between the generated THz wave and the pump beam is

$$\theta = \arcsin(v_p^{pol}/v_g^{pump}) \qquad (4)$$

and the corresponding polariton forward component is

$$\varphi = \arccos(v_p^{pol}/v_g^{pump}) \qquad (5)$$

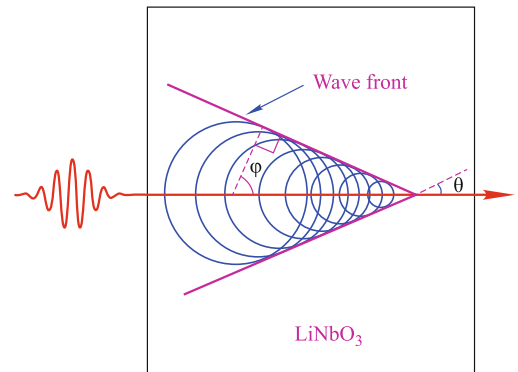Here v_p^{pol} is the polariton phase velocity, and v_g^{pump} is the pump group velocity [28].

Fig. 3 A focused femtosecond laser pulse generates a Cherenkov radiation cone of THz phonon polariton. The laser pulse propagates along the arrow direction from the input face of a LiNbO$_3$ crystal to the output face.

3.2 In bulk crystal

Here we introduce the propagation of THz phonon polariton in bulk crystal using a typical setup that femtosecond laser pulses are focused into a bulk uniaxial ferroelectric LiNbO$_3$ by a cylindrical lens, as shown in Fig.

4. Both the polarization of the pump pulse (red) and the generated phonon polariton wave (blue) are along the crystal optical axis (z axis of the coordinate system). THz phonon polariton wave propagates in the crystal with a Cherenkov angle.
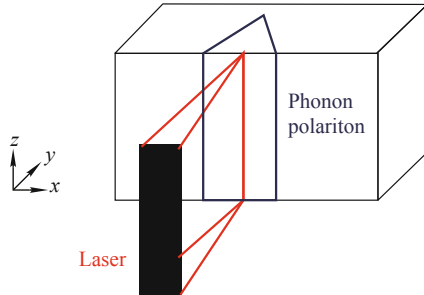

Fig. 4 Typical setup for THz phonon polariton wave generated in a LiNbO₃ crystal by a femtosecond laser pulse and the coordinate system. The pump laser pulse (red) propagates through the crystal, orthogonal to the crystal surface, while the THz phonon polariton waves propagate with a Cherenkov angle.

In the top view of the crystal (x–y plane), a Cherenkov-like propagation can be clearly observed, as shown in Fig. 5. There are simulation results using Finite Element Method (FEM). These pictures illustrate that the phonon polariton are generated and propagate when the excitation pulse traverses the sample from front to back. The sample is a 0.5 mm³ LiNbO₃ crystal. A 100 fs, 800 nm laser pulse is focused to a 20 μm width line into the sample.
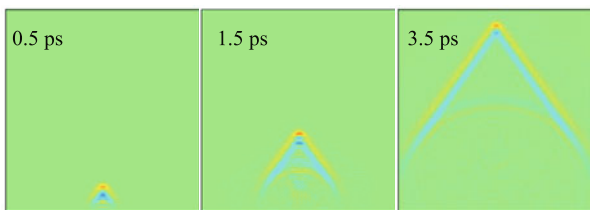

Fig. 5 Top view (x–y plane) of the generation and propagation process of phonon polariton. A 100 fs, 800 nm laser pulse is focused to a 20 μm width line into a 0.5 mm³ LiNbO₃ crystal to excite the broadband polariton wave. The snapshots are the results of 0.5, 1.5, and 3.5 ps, respectively.

From the front view (x–z plane), the THz phonon poalriton waves propagate almost perpendicular to the pump beam and primarily in the lateral directions, as shown in Fig. 6.

The propagating waveform of THz phonon polariton induces a change of the refractive index of the sample through electro–optic effect. And for its specular property that it propagates primarily in the lateral directions as shown in Fig. 6, it is possible to obtain time-resolved images of the electric field of the phonon polariton. The time-delayed probe pulses (400 nm), which can be expanded to illuminate the whole sample and propagate
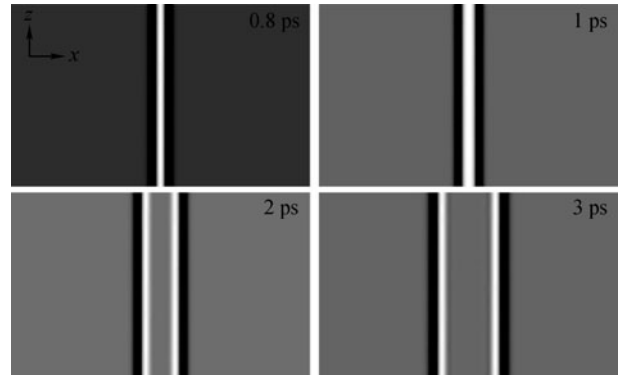

Fig. 6 Two dimensional plots of the front view (x–z plane). A 50 fs, 800 nm pump laser is focused to a 30 μm line into a LiNbO₃ crystal. Reproduced from Ref. [34].

parallel to the pump beam, experience a spatially dependent phase shift proportional to the refractive index change. These phase information are transformed to amplitude information, which can be detected by a CCD camera, using some methods. We will introduce and compare these methods in the following section. For the imaging in bulk crystal, the method widely used is Talbot effect, where the CCD camera is slightly shifted out of imaging plane, as shown in Fig. 7. The series of images can construct a "movie" that fully captures the spatiotemporal evolution of phonon polariton in the sample.
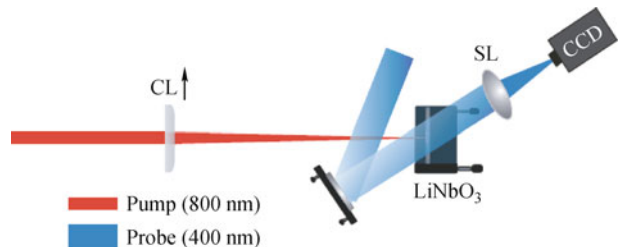

Fig. 7 Imaging setup of THz phonon polariton in a bulk LiNbO₃ crystal. CL: Cylindrical lens, SL: Spherical lens. Reproduced from Ref. [27].

Using this imaging technique, the researchers have gotten the spatiotemporal images of phonon polariton [25, 26, 40, 41], coherent controlled polatiton generation and propagation [42–45], and integrated functional elements in the crystal [46–51]. Even a research field of "photonics" analogous to photonics and electronics is brought out, in which signals are carried by phonon polariton to bridge the gap between electronics and photonics [27, 29, 52].

3.3　In thin crystal

Although the imaging in bulk crystal has gotten fruitful results, there are some drawbacks that prevent it from being more widely applicable. One limitation is that the

probe beam is not phase matched to the excitation for the difference of refractive index ($n_e = 2.163$, 2.312 for 800 nm and 400 nm in LiNbO$_3$ respectively). But in sufficiently thin crystal (typically thinner than 300 μm), the phase-matching condition on probing is relaxed since any differences in the propagation times for pump and probe pulses through so thin crystal can be negligible.

The other drawback is the imaging technique using Talbot effect in bulk crystal, which converts the phase information to intensity information for the detection of CCD camera. But only certain wave vector components of the phase image can be efficiently converted to the intensity information from the deduction of Fresnel diffraction theory [53, 54]. And at the same time static structures in the sample will be blurred because the CCD camera is translated out of the image plane of the sample. In this section, we will introduce some new methods in thin crystal to address this problem.

Moreover, the thin ferroelectric crystal can be used for an integration platform, not only for THz wave but also for the interconversion between terahertz and optical or electrical signal. Furthermore, when the sample thickness becomes subwavelength, the strong evanescent field of the THz wave can interact with materials deposited on the crystal surface. This opens the door for the interface of the ferroelectric crystal with other optical or photoelectric devices.

Because of these advantages, most work of THz phonon polariton is focused on the subwavelength ferroelectric crystal now. In this section, we will introduce it in more detail.

The common part of the experimental setups described below is a pump probe system, as shown in Fig. 8. The laser is a Ti:sapphire regenerative amplifier, whose pulse duration is about 100 fs, central wavelength is 800 nm, and repetition rate is 1 kHz. The laser pulses are split to pump and probe, which can be delayed relative to one another. The pump is focused into the sample (LiNbO$_3$, LN) at normal incidence using a cylindrical lens (CL) to produce a line source of THz phonon polariton. The

generation process of THz phonon polariton is similar to that in Fig. 4 and the coordinate system is also the same to Fig.4. For optimum signal, the polarization of pump and generated THz fields are all parallel to the optical axis of LiNbO$_3$. The probe is frequency-doubled to 400 nm through a BBO crystal. It is spatially filtered to minimize the spatial variation noise and expanded to be larger than the sample. It is collinear with the pump reflected by a dichroic mirror. So the generated THz phonon polariton wave travels in the crystal plane orthogonal to the direction of probe propagation, as shown in Fig. 9.

Fig. 9 The pump probe geometry in LiNbO$_3$ crystal. The 800 nm and 400 nm beams propagate through the crystal, orthogonal to its surface. THz phonon polariton waves propagate in the plane of the waveguide, orthogonal to the probe.

Because LiNbO$_3$ is an electro–optic crystal, the THz electric field can modulate the refractive index significantly. The probe beam experiences a spatially dependent phase shift proportional to the refractive index change when it passes through the sample. So the signal of THz phonon polariton is codded into the phase of probe beam. But the normal detector, such as a CCD camera, is intensity detector, which cannot detect phase signal directly. Therefore, a method is needed to convert the phase information to amplitude information.

Before the introduction of these methods, which can change the phase information to the intensity
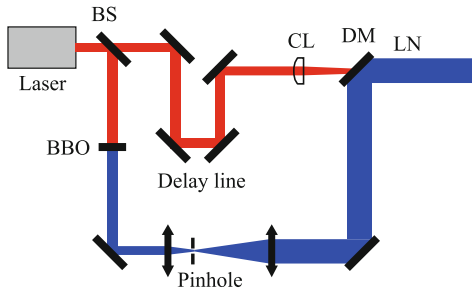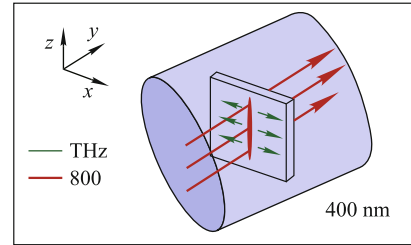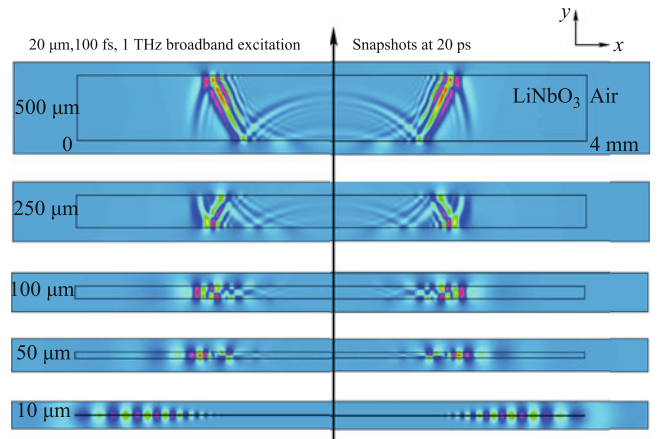

Fig. 8 The pump probe setup for THz phonon polariton imaging. The laser is a Ti:sapphire regenerative amplifier. BS is partial beam splitter, CL is cylindrical lens, and DM is dichroic mirror. LN is the sample LiNbO$_3$.

Fig. 10 Waveguide confinement effect for THz phonon polariton over crystal thickness. The arrow means the incidence direction of pump beam. Reproduced from Ref. [34].

information, the confinement effect of the thin sample is shown in Fig. 10.

The excitation conditions are the same to what mentioned above. In 500 μm thickness sample, the wave experiences two bounces which induce the interference pattern. In this case, the properties of phonon polariton is similar to that in bulk crystal. But in 10 μm crystal, the wave is quickly straightened out and propagates with no interference pattern. The simulation results show that the propagation properties of THz phonon polariton are changed from bulk regime to waveguide regime as the crystal thickness is gradually decreased.

The methods, which can generate in-focus images and quantitatively measure the electric field of THz phonon polariton in large-area or structured samples, are phase contrast and self-compensating polarization gating imaging [54, 55]. Phase contrast imaging, introduced by Frits Zernike in the 1930s [56, 57], has been widely used for the imaging of transparent samples in biology. Here, we used a 4f system, with a phase plate at the center of the focal plane of the first lens, to implement this technique, shown in Fig. 11. The phase mask induces a $\pi/2$ relative phase shift between the zeroth order beam and the diffracted light. When these two fields are recombined on the CCD camera (image plane), the phase image is converted to intensity image.

The generation and propagation process of THz phonon polariton in the thin crystal can be gotten using the pump probe setup in Fig. 8 to generate a movie. Figure 12(a) shows a snapshot of the movie, 42 ps after THz phonon polariton is generated. It is broken up into discrete modes for the confinement effect of the waveguide.
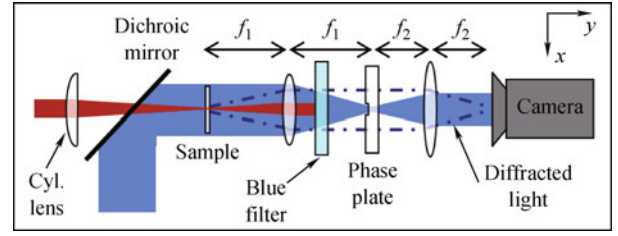

Fig. 11 Experimental setup of phase contrast imaging. The pump (red) and probe (blue) beams come from the laser as that in Fig. 8. $f_1 = f_2 = 15$ cm. Reproduced from Ref. [54].

Because we use a cylindrical lens to excite THz phonon polariton, the signal of Fig. 12(a) can be averaged over the vertical dimension and changed to the signal of the electric field of THz phonon polariton, shown in Fig. 12(b).
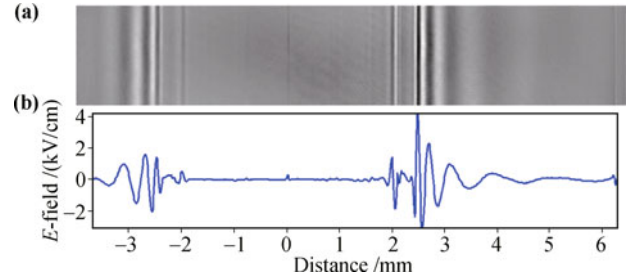

Fig. 12 (a) Image of THz phonon polariton 42 ps after it is generated. The chirping of the pulse because of waveguide dispersion. (b) The electric field profile from (a). Reproduced from Ref. [54].

We repeat the treatment step as mentioned above for the movie, and place the results in one row of matrix, as shown in Fig. 13(a). It fully shows the temporal and spatial evolution of THz phonon polariton. In this image, dispersion, reflection, interference, and the different
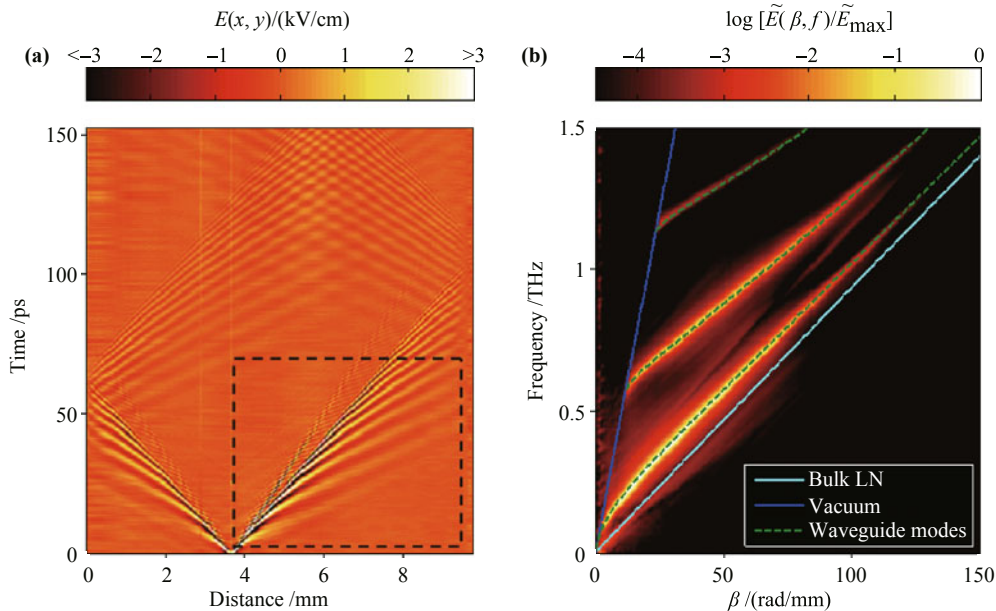

Fig. 13 (a) E-field evolution of THz phonon polariton as a function of space and time. The sides of the image are the crystal edges. (b) 2-dimensional Fourier transform of the boxed region in (a). The red curves are the experimental results, and the other cures are the calculation results. Reproduced from Ref. [54].
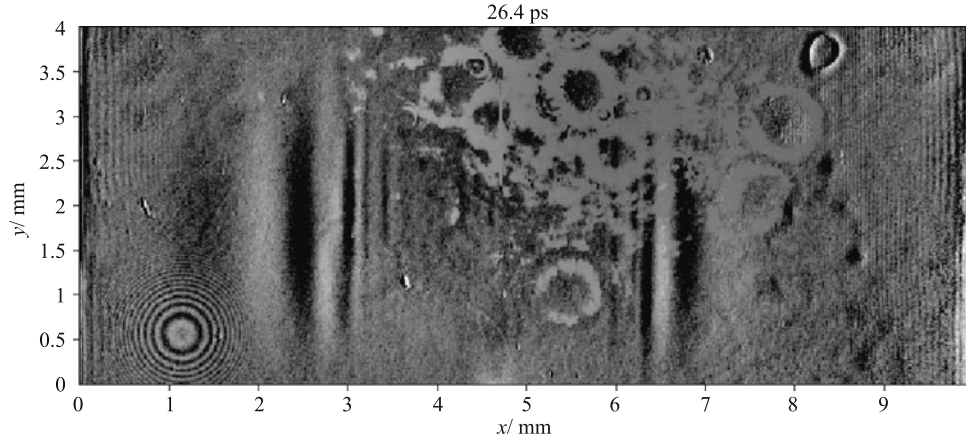
Fig. 14 Image of the phonon polariton 26.4 ps after it is generated, using normal polarization gating setup. Two crystals with the same thickness are put with the optical axis perpendicular with each other.

waveguide modes are all clearly apparent. Figure 13(b) is the 2-dimensional Fourier transform of image (a), which shows the dispersion of the waveguide modes.

Polarization gating has been used in ultrafast optics for a long time, especially through optical Kerr effect or electro–optic sampling. It was also used for THz phonon polartion imaging [53]. But the inherent birefringence of LiNbO$_3$ is large, which is mixed with the transient birefringence induced by THz phonon polariton. The phase shift induced by THz phonon polariton is small and dynamic, so it is hard to get good signal in large or structured samples. We also try to compensate the inherent birefringence using a second crystal of equal thickness with its optic axis rotated by 90 degree. However, the defects and non-uniformity of the thickness make it impossible. Figure 14 shows the result. If a structured sample is considered, it will be an impossible mission.

To address this problem, we improve the setup to be self-compensating, in which the probe beam goes through the crystal twice with flipped vertical and horizontal polarizations to compensate the inherent birefringence by the sample itself. The experimental setup is shown in Fig. 15. A 4f system is also used here. The retroreflective mirror (RM) reflects the image of the crystal through itself with a magnification of 1. The probe beam double passes through the quarter wave plate (QW1), whose fast axis rotated to 45°. So QW1 flips the vertical and horizontal polarizations of probe beam. After the second pass through the sample, the spatially varying phase shift between the vertical and horizontal polarization components from the first pass is compensated. In this way, the crystal self-compensates any phase shift introduced by the inherent birefringence or any defects, which only induce birefringence phase shift. Figure 16 shows the noises induced by phase defects in the image, which are compensated by self-compensating setup. At the same time, the phase shift induced by THz

phonon polariton is not compensated, because it is generated only after the probe pulses pass through the sample at the first time.
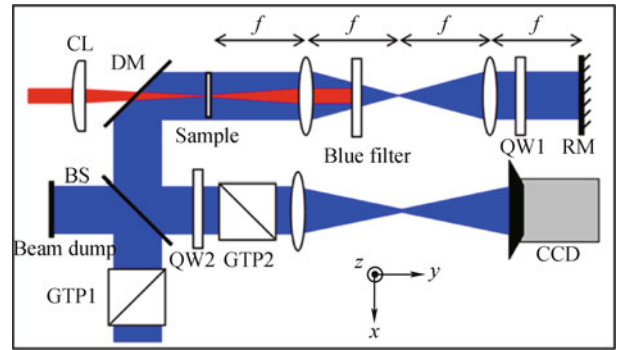

Fig. 15 Experimental setup of self-compensating polarization gating. The pump (*red*) and probe (*blue*) beams come from the laser as that in Fig. 8. GTP1 and GTP2 are Glan–Taylor prisms, whose polarizations are at +45° and –45° to *z*-axis respectively. BS: 400 nm beam splitter; CL: Cylindrical lens; DM: Dichroic mirror; RM: Retroreflective mirror. QW1 and QW2 are zero order 400 nm quarter-wave plates with optic axes at +45° and parallel to *z*-axis respectively. Reproduced from Ref. [58].

Although the setup of self-compensating polarization gating is complicated, it can also be used for the imaging of structured crystal, just like phase contrast setup. Figure 17 shows an image, picked up from a movie, 56 ps after THz phonon polariton wave is generated and guided to a Y-coupler. The Y-coupler is structured in a LiNbO$_3$ crystal using femtosecond laser machining.

The other two methods for imaging of THz phonon polariton were compared with phase contrast and self-compensating polarization gating in detail [53, 55]. Figure 18 shows the space-time plots, similar to Fig. 13(a), for each imaging method. For Sagnac interference method, there are some diffraction patterns from the edge of the crystal because the distances of two interference beam are different. The Talbot imaging just shows a part of information as we discussed above.
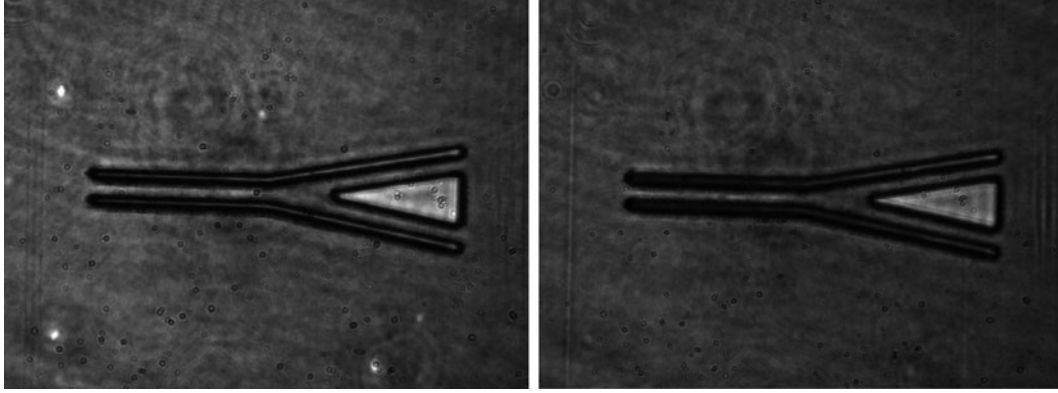
Fig. 16 Defects in LiNbO$_3$ crystal induce birefringence phase shift noise in the image (left), and that are compensated by self-compensating setup (right).
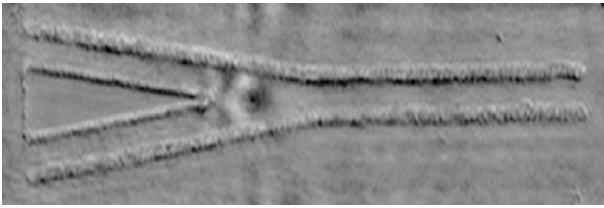

Fig. 17 Self-compensating polarization gating imaging shows THz phonon polariton wave guided in a Y-coupler, which is structured into a LiNbO$_3$ crystal using femtosecond laser machining.
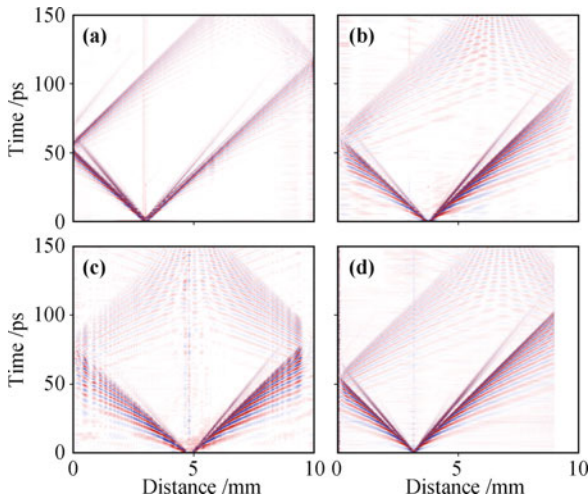

Fig. 18 *E*-field evolution of THz phonon polariton as a function of space and time. **(a)** Talbot imaging. **(b)** Phase contrast imaging. **(c)** Sagnac interference imaging. **(d)** Polarization gating imaging. Reproduced from Ref. [55].

Figure 19 shows the average wave vector response for each imaging method. Both phase contrast and polarization gating have smooth and un-modulated wave vector response and large detection bandwidths. So they are better than Sagnac and Talbot imaging.

As a conclusion from the analytical and experimental comparison, both phase contrast and self-compensating gating can focus in images and quantitatively measure the THz phonon polariton in large or structured sample. Of these two methods polarization gating has better
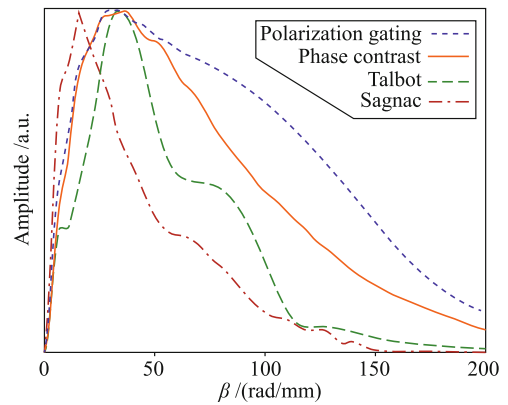

Fig. 19 Measured wave vector content of the images for different imaging methods. Reproduced from Ref. [55].

signal-to-noise ratio and is preferred for most situations, while phase contrast imaging has better spatial resolution and is preferred for measurements in structured samples. More details for the comparison of these four methods can be found in Refs. [53, 55].

4 Properties of subwavelength waveguide of THz phonon polariton

As discussed above, the thin crystal is necessary for the in-focus quantitative imaging of THz phonon polariton and the integration platform. We have experimentally and theoretically analyzed the properties of generation and propagation of THz phonon polariton in the subwavelength, anisotropic LiNbO$_3$ crystal.

Figure 20 shows dispersion curves for different propagation directions of THz phonon polariton.

From our experimental and simulation results, we can get a series of phase or group effective refractive index ellipses of different modes. They are useful to exposit the propagation properties of THz phonon polariton and are necessary for the future research of nonlinear phonon polariton. For example, Figure 21 shows a phase effective
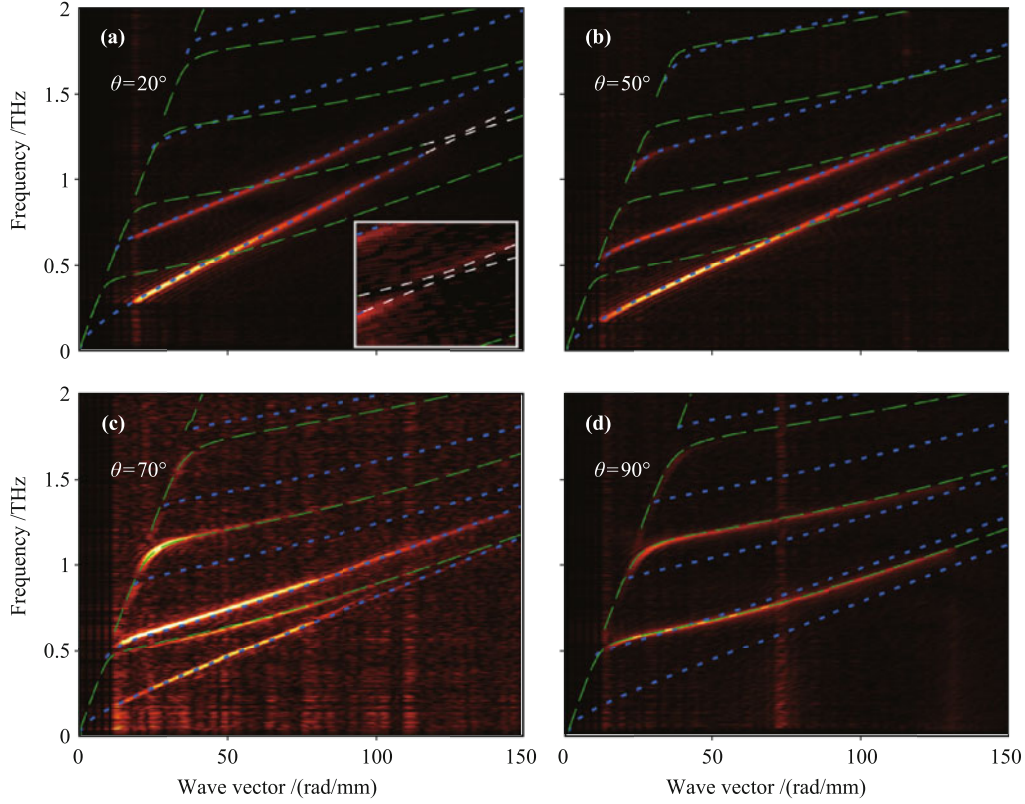
Fig. 20 Dispersion curves for different propagation directions. Blue and green dotted lines are calculated TE-like and TM-like modes, respectively. All the experimental results agree well with the calculated curves. Reproduced from Ref. [58].

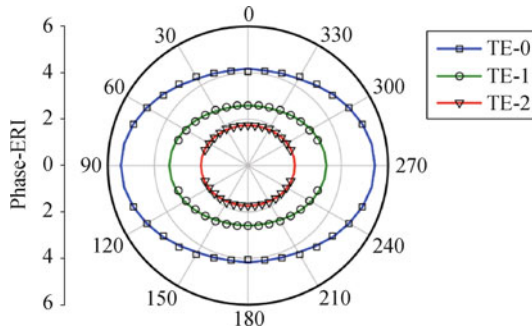refractive index ellipse for the first three TE-like modes at wave vector 50 rad/μm.

Fig. 21 Effective refractive index ellipse for three TE modes at a wave vector 50 rad/mm in a 50 μm LiNbO$_3$ slab waveguide. The solid lines are the calculated results. The open symbols are experimental data. Reproduced from Ref. [58].

5   Summary and perspectives

In this article, we mainly demonstrate the imaging of THz phonon polariton, which is generated by femtosecond laser through ISRS effect in ferroelectric crystal. We pay more attention to the imaging in thin crystal, which can be used as an integration platform of THz phonon polariton or an interconversion of terahertz, op-

tical, and electrical signals. The imaging techniques of phase contrast and self-compensating polarization gating have been introduced in more detail. These techniques all can get the quantitatively time-resolved in-focus imaging of THz phonon polariton in large or structured samples. We also introduce the properties of subwavelength, anisotropic waveguide for THz phonon polariton. They are usually thin ferroelectric crystals, which are the important platforms for the research of THz phonon polariton and for the integrated terahertz-optics or terahertz-electrics.

Thus, we brought out the detection techniques and properties of research platform of THz phonon polariton. An enhanced frequency-tunable source of THz phonon polariton was also achieved in a LiNbO$_3$ slab waveguide [22]. So as an important member of elementary excitation family, THz phonon polariton is very significant for both theoretical research and practical applications. One of them is polaritonics, the integrated platform, especially the subwavelength waveguide deposited with metamaterials or nanoparticles. Because of the strong evanescent field, the intensive interaction may bring new ideas for the integrated terahertz-optics. The other is to illustrate the principles of electromagnetism for the excellent spatiotemporal resolution of the imaging. Another application is to coherent control lattice vibration.

It is very interesting not only for nonlinear terahertz spectroscopy and terahertz nonlinear optics, but also for nonlinear phonon polariton.

References

1. K. Huang, Proc. Roy. Soc., 1951, 208(1094): 352

2. M. Born and K. Huang, Dynamical Theory of Crystal Lattices, London: Oxford University Press, 1954

3. D. Pines, Elementary Excitation in Solids, New York: W. A. Benjamin, 1964

4. S. Nakajima, Y. Toyozawa, and R. Abe, The Physics of Elementary Excitations, Springer series in solid-state sciences, Berlin: Springer, 1980

5. K. Huang, Nature, 1951, 167(4254): 779

6. J. J. Hopfield, Phys. Rev., 1958, 112(5): 1555

7. C. H. Henry and J. J. Hopfield, Phys. Rev. Lett., 1965, 15(25): 964

8. Z. Gan, Physics, 2009, 38: 581 (in Chinese)

9. Y. Shen and N. Bloembergen, Phys. Rev., 1966, 143(2): 372

10. A. Imamog, R. Ram, S. Pau, and Y. Yamamoto, Phys. Rev. A, 1996, 53: 4250

11. H. Deng, G. Weihs, C. Santori, J. Bloch, and Y. Yamamoto, Science, 2002, 298(5591): 199

12. M. Richard, J. Kasprzak, R. André, R. Romestain, L. S. Dang, G. Malpuech, and A. Kavokin, Phys. Rev. B, 2005, 72(20): 201301

13. J. Kasprzak, M. Richard, S. Kundermann, A. Baas, P. Jeambrun, J. Keeling, F. M. Marchetti, M. H. Szymanska, R. Andre, J. L. Staehli, V. Savona, P. B. Littlewood, B. Deveaud, and L. S. Dang, Nature, 2006, 443(7110): 409

14. S. A. Maier, Plasmonics: Fundamentals and Applications, Berlin: Springer, 2007

15. W. Hayes and R. Loudon, Scattering of Light by Crystals, New York: John Wiley & Sons, 1978

16. D. H. Auston, Appl. Phys. Lett., 1983, 43(8): 713

17. D. H. Auston, K. P. Cheung, J. A. Valdmanis, and D. A. Kleinman, Phys. Rev. Lett., 1984, 53(16): 1555

18. D. Kleinman and D. Auston, IEEE J. Quantum Electron., 1984, 20(8): 964

19. K. P. Cheung and D. H. Auston, Phys. Rev. Lett., 1985, 55(20): 2152

20. D. H. Auston and M. C. Nuss, IEEE J. Quantum Electron., 1988, 24(2): 184

21. K. L. Yeh, M. C. Hoffmann, J. Hebling, and K. A. Nelson, Appl. Phys. Lett., 2007, 90(17): 171121

22. K. Lin, C. Werley, and K. Nelson, Appl. Phys. Lett., 2009, 95(10): 103304

23. Z. Chen, X. Zhou, C. A. Werley, and K. A. Nelson, Appl. Phys. Lett., 2011, 99(7): 071102

24. J. Hebling, M. C. Hoffmann, H. Y. Hwang, K. L. Yeh, and K. A. Nelson, Phys. Rev. B, 2010, 81(3): 035201

25. R. M. Koehl, S. Adachi, and K. A. Nelson, J. Phys. Chem. A, 1999, 103(49): 10260

26. R. M. Koehl, S. Adachi, and K. A. Nelson, J. Chem. Phys., 1999, 110(3): 1317

27. D. W. Ward, Polaritonics: An Intermediate Regime between Electronics and Photonics, Boston: Massachusetts Institute of Technology, 2005

28. E. R. Statz, Phonon polariton interaction with patterned materials, Boston: Massachusetts Institute of Technology, 2008

29. C. A. Werley, THz Polaritonics: Optical THz Generation, Detection, and Control on a Chip, Boston: Massachusetts Institute of Technology, 2012

30. L. Dhar, J. A. Rogers, and K. A. Nelson, Chem. Rev., 1994, 94(1): 157

31. Y. X. Yan, Gamble, and K. A. Nelson, J. Chem. Phys., 1985, 83(11): 5391

32. Y. X. Yan and K. A. Nelson, J. Chem. Phys., 1987, 87(11): 6240

33. Y. X. Yan and K. A. Nelson, J. Chem. Phys., 1987, 87(11): 6257

34. Z. Chen, Modeling Phonon-Polariton Generation and Control in Ferroelectric Crystals, Boston: Massachusetts Institute of Technology, 2009

35. C. Yang, Study on Ultrafast Imaging and Propagation Characteristics of Terahertz Phonon Polariton, Tianjin: Nankai University, 2011 (in Chinese)

36. T. P. Dougherty, G. P. Wiederrecht, and K. A. Nelson, J. Opt. Soc. Am. B, 1992, 9(12): 2179

37. C. A. Werley, K. Fan, A. C. Strikwerda, S. M. Teo, X. Zhang, R. D. Averitt, and K. A. Nelson, Opt. Express, 2012, 20(8): 8551

38. T. E. Stevens, J. K. Wahlstrand, J. Kuhl, and R. Merlin, Science, 2001, 291(5504): 627

39. J. K. Wahlstrand and R. Merlin, Phys. Rev. B, 2003, 68(5): 54301

40. T. Feurer, N. S. Stoyanov, D. W. Ward, and K. A. Nelson, Phys. Rev. Lett., 2002, 88(25): 257402

41. N. S. Stoyanov, D. W. Ward, T. Feurer, and K. A. Nelson, J. Chem. Phys., 2002, 117(6): 2897

42. R. M. Koehl and K. A. Nelson, Chem. Phys., 2001, 267(1–3): 151

43. R. M. Koehl and K. A. Nelson, J. Chem. Phys., 2001, 114(4): 1443

44. T. Feurer, J. C. Vaughan, and K. A. Nelson, Science, 2003, 299(5605): 374

45. T. Feurer, J. C. Vaughan, T. Hornung, and K. A. Nelson, Opt. Lett., 2004, 29(15): 1802

46. N. S. Stoyanov, D. W. Ward, T. Feurer, and K. A. Nelson, Nat. Mater., 2002, 1(2): 95

47. N. S. Stoyanov, T. Feurer, D. W. Ward, and K. A. Nelson, Appl. Phys. Lett., 2003, 82(5): 674

48. N. Stoyanov, T. Feurer, D. Ward, E. Statz, and K. Nelson, Opt. Express, 2004, 12(11): 2387

49. D. W. Ward, J. D. Beers, T. Feurer, E. R. Statz, N. S. Stoyanov, and K. A. Nelson, Opt. Lett., 2004, 29(22): 2671

50. D. W. Ward, E. R. Statz, and K. A. Nelson, Appl. Phys. A, 2007, 86(1): 49

51. E. Statz, K. H. Lin, K. Nelson, M. Yang, and K. Webb, Opt. Lett., 2010, 35(17): 2931

52. T. Feurer, N. S. Stoyanov, D. W. Ward, J. C. Vaughan, E. R. Statz, and K. A. Nelson, Annu. Rev. Mater. Res., 2007, 37(1): 317

53. P. Peier, S. Pilz, F. Müller, K. A. Nelson, and T. Feurer, J. Opt. Soc. Am. B, 2008, 25(7): 70

54. Q. Wu, C. Werley, K. Lin, A. Dorn, M. Bawendi, and K. Nelson, Opt. Express, 2009, 17(11): 9219

55. C. A. Werley, Q. Wu, K. H. Lin, C. R. Tait, A. Dorn, and K. A. Nelson, J. Opt. Soc. Am. B, 2010, 27(11): 2350

56. F. Zernike, Science, 1955, 121(3141): 345

57. F. Zernike, Physica, 1942, 9(7): 686

58. C. Yang, Q. Wu, J. Xu, K. A. Nelson, and C. A. Werley, Opt. Express, 2010, 18(25): 26351